

Band gap tuning of epitaxial SrTiO_{3-δ}/Si(001) thin films through strain engineering

Ryan J. Cottier, Nathan A. Steinle, Daniel A. Currie, and Nikoleta Theodoropoulou^{a)} *Physics Department, Texas State University, San Marcos, Texas 78666, USA*

(Received 24 July 2015; accepted 15 November 2015; published online 1 December 2015)

We investigate the effect of strain and oxygen vacancies (V_O) on the crystal and optical properties of oxygen deficient, ultra-thin (4–30 nm) films of $SrTiO_{3-\delta}$ (STO) grown heteroepitaxially on p-Si(001) substrates by molecular beam epitaxy. We demonstrate that STO band gap tuning can be achieved through strain engineering and show that the energy shift of the direct energy gap transition of $SrTiO_{3-\delta}/Si$ films has a quantifiable dimensional and doping dependence that correlates well with the changes in crystal structure. © 2015 AIP Publishing LLC. [http://dx.doi.org/10.1063/1.4936608]

Oxide heterostructures and surfaces have attracted considerable attention in recent years due to the discovery of two dimensional electron gases (2DEG), superconductivity, and quantum confinement. The physical properties of these interfaces can be controlled through carrier manipulation using polar discontinuities, band bending, doping, epitaxial strain, and stoichiometry.

SrTiO_{3-δ} (STO) is a diverse and highly controllable material and has been studied extensively. Bulk STO has a perovskite structure and is a wide band gap insulator with an indirect band gap of 3.2 eV.4 It has a large dielectric constant that is temperature, frequency, and electric field dependent,⁵ making it potentially suitable for a range of applications. Further, strain engineering of STO can be achieved with lattice mismatch through substrate choice, doping, or stoichiometric variations, all of which can alter the crystal structure and electronic properties. Additionally, STO becomes conductive when doped with Nb or La or when oxygen vacancies (V_O) are induced.^{6,7} These V_O in STO can generate electrons as conduction carriers and can cause blue light emission at room temperature (RT) when induced through Ar⁺ irradiation.⁸ However, V_O are also known to increase the leakage current in STO-based devices, thus limiting their suitability for many applications.

STO can be integrated with Si and the STO/Si heterostructure has been used as a virtual substrate for oxide growth. The heteroepitaxy of STO on Si is rather challenging because of the high reactivity of Si with $\rm O_2$, 10 but it has been demonstrated that STO can be grown epitaxially on Si(001) through a 45° rotation of the STO unit cell with respect to Si resulting in a 1.7% compressive strain. $^{11-13}$

Although STO is paraelectric, ultrathin STO films become ferroelectric at $T=300\,\mathrm{K}$ for sufficiently large biaxial strains induced by epitaxial growth either on Si or other oxide substrates. ^{13,14} Ferroelectricity in 100 nm, O₂ deficient, tetragonal STO homoepitaxial films has been also reported at $T=300\,\mathrm{K}$. ¹⁵

In this report, we investigate the effects of strain and $V_{\rm O}$ on the lattice constant and optical properties of ultrathin STO (4-60 nm) films grown heteroepitaxially on p-Si(001)

a)ntheo@txstate.edu

substrates under different O_2 pressures, $P(O_2)$, and demonstrate that band gap tuning through strain engineering by varying the STO film thickness (d) and V_O . No post-growth anneals were performed, preventing the formation of a SiO₂ interfacial layer and contrasting this study from earlier reports of 50–100 nm thick STO/Si films with a SiO₂ interfacial layer. The dielectric function is measured using spectroscopic ellipsometry (SE), and for a thin (d= 4.5 nm), highly strained film, a maximum blueshift of 250 \pm 30 meV is observed in the first direct energy transition (E_{di}) compared to the STO bulk value of 3.75 eV. This blueshift decreases with either an increase in d or a decrease in V_O .

The STO/Si samples were grown by molecular beam epitaxy (MBE) using a growth procedure reported elsewhere 18,19 in a 3 in. DCA Instruments M600 system. Reflection high energy electron diffraction (RHEED) was used to monitor the surface quality and stoichiometry, and, due to the strong reactivity of Sr with O_2 , the Sr flux had to be adjusted for each $P(O_2)$ and all films were Ti-terminated.

All films were characterized by XRD using a Bede D1, and *d* and root mean square roughness (RMS) were determined using x-ray reflectivity (XRR) and the Bede REFS software package. ^{20,21} Topography and RMS were measured with a Veeco Dimension 3100 atomic force microscope (AFM), and the carrier density and mobility were determined through Hall measurements. The RT optical properties of STO/Si were measured using a Woolam M-2000 Variable Angle SE (VASE) at angles of 45°–70°, photon energy of 1.5–6.0 eV, and 10 meV steps.

Two sets of samples are investigated: Set A consists of STO/Si thin films grown under the exact same conditions, $T_S = 500 \,^{\circ}\text{C}$, $P(O_2) = 4 \times 10^{-8} \,^{\circ}\text{Torr}$, but with $d: 4.2–30 \,\text{nm}$. Set B consists of STO/Si grown at $T_S = 500 \,^{\circ}\text{C}$, $d = 9.0 \pm 0.5 \,^{\circ}\text{nm}$, and $P(O_2)$ varied from 4×10^{-8} to $4 \times 10^{-7} \,^{\circ}\text{Torr}$.

Fig. 1(a) shows 2θ - ω XRD survey scans for three films from Set A with d=4.5, 8.6, and 14.8 nm. Only STO(001) and (002) peaks are present. No other orientations or phases were detected other than peaks attributable to the Si substrate (and the X-ray source emitting not only by Cu K_{α} , but also Cu K_{β} and W L_{α}). The dashed line corresponds to the Bragg reflection from bulk STO(002). Because of the lattice mismatch, the STO(002) peak shifts to lower angles for thin

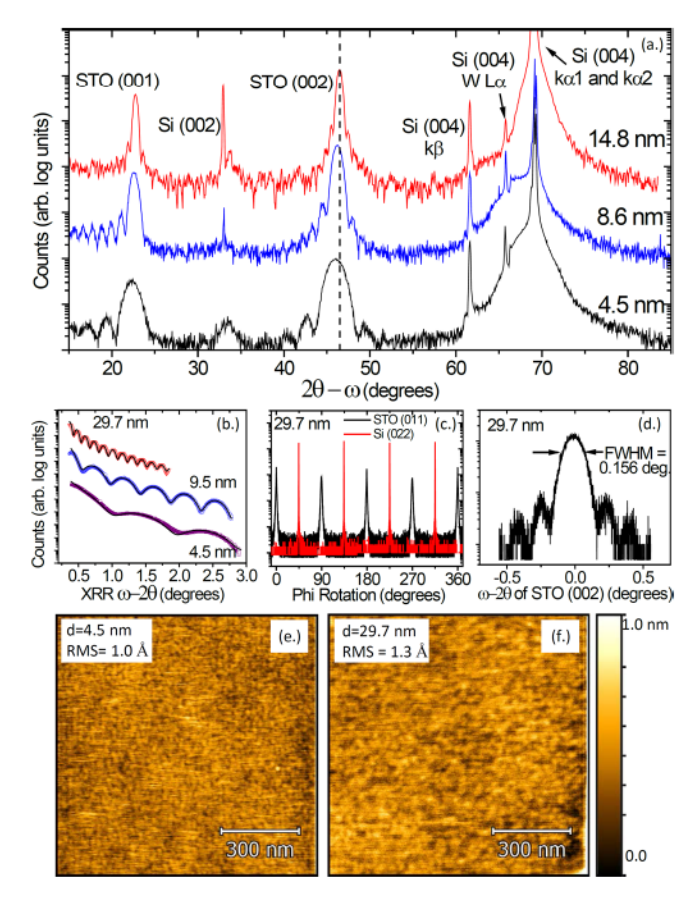


FIG. 1. (a) 2θ - ω XRD survey scan of three films of STO/Si(001) grown at $P(O_2) = 4 \times 10^{-8}$ Torr. (b) XRR with fitted curves overlaid in black were used to determine d. (c) Off-axis Φ -scan of the STO(011) and Si(022) peaks demonstrating a single in-plane orientation of the 29.7 nm STO film. (d) STO(002) rocking curve for a 29.7 nm film. (e) and (f) Contact AFM topographical images of the 4.5 and 29.7 nm films showing an RMS of

films and approaches the bulk value as d increases and the lattice relaxes. The samples' Si(004) substrate peaks were aligned, and the shift of the STO(002) film peak relative to bulk was measured for both sets. Fig. 1(d) shows an ω -2 θ high-resolution scan around STO(002) for d = 29.7 nm with a full width half maximum (FWHM) of 0.156°, very close to the calculated Scherrer value of 0.142°, confirming the high crystalline quality of the films.²² Epitaxy is demonstrated in the Φ -scan (Fig. 1(c)) taken of the STO(011) and Si(022) planes, showing clear 4-fold symmetry and a 45° in-plane rotation of STO with respect to Si. Additionally, d and RMS were determined by fitting the measured XRR data (Fig. 1(b), fittings overlaid). The films were atomically flat with RMS of 0.295 nm, 0.321 nm, and 0.35 nm for the 29.7 nm, 9.6 nm, and 4.5 nm films, respectively. These results were also verified by AFM as shown in Figs. 1(e) and 1(f) for the 4.5 nm and 29.7 nm films with a measured typical RMS of less than 0.2 nm.

As reported earlier, the 1.7% compressive strain between the STO film and Si is accommodated by an out-of-plane expansion, reducing the symmetry from cubic m3m to tetragonal 4/mm, thus increasing in the tetragonality (c_s/a_s) , where a_s and c_s are the in-plane and out-of-plane lattice constants of the film). For the 4.5 nm sample, c = 3.960 Å (Fig. 2(a), left axis) corresponding to 1.5% strain. As d increases, c and strain decrease through the formation of dislocations,

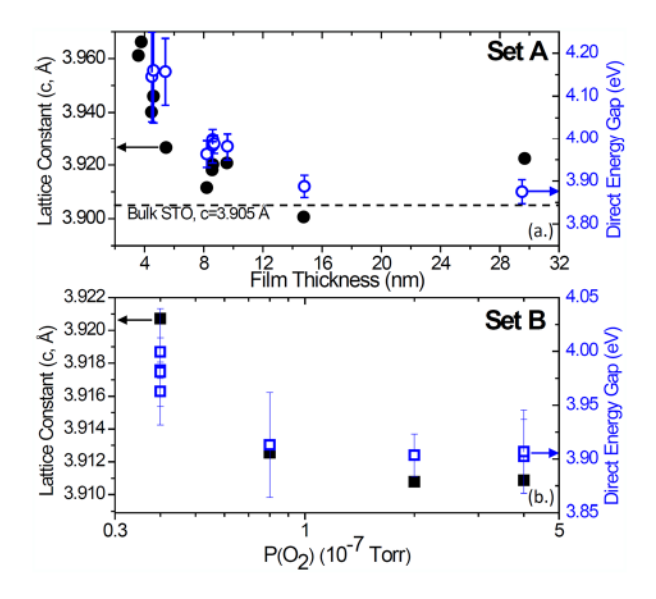


FIG. 2. Out of plane lattice constant, c, calculated from XRD. (a) c (left-axis) and E_{di} (right-axis) vs. d for Set A. (b) c (left-axis) and E_{di} (right-axis) vs. $P(O_2)$ Set B.

and for d = 15 nm, c = 3.905 Å, the value for bulk STO, indicating that the film is fully relaxed, consistent with earlier results.¹⁵

Fig. 2(b) (left axis) shows the increase in c with V_O for Set B grown at $P(O_2) = 4 \times 10^{-8} - 4 \times 10^{-7}$ Torr. To quantify the oxygen deficiency, δ , we measured a sheet carrier concentration, $n_s \approx 5 \times 10^{13} \text{ cm}^{-2}$ for d = 9 nm film grown at $P(O_2) = 4 \times 10^{-8}$ Torr corresponding to $\delta \approx 0.05\%$, assuming that each Vo contributes two electrons in SrTiO_{3-δ}. For the films grown at $P(O_2) = 4 \times 10^{-7}$ Torr, $\delta \approx 0.005\%$. Strain and c increase with Vo, with c changing from 3.911 to 3.921 Å. Such an increase has been reported for STO films grown by Pulsed Laser Deposition (PLD) at low P(O2) on STO and SrRuO₃ (SRO) substrates 15,23 and in bulk STO substrates that were reduced (annealed in UHV).24 In agreement with our results, a decrease of c from 3.92 to 3.905 Å was observed for 20 nm STO films grown on LaAlO3 (LAO) by Laser-MBE when $P(O_2)$ was changed by an order of magnitude. 25 The increase in c, and thus the tetragonality, is associated with RT ferroelectricity. 15 Theoretical calculations 26 predict a transformation from a paraelectric tetragonal phase to a non-centrosymmetric ferroelectric phase for films with an in-plane compressive strain greater than -0.75% due to the strong coupling of strain and polarization.²⁷ A c/a ratio of 1.02 for a 4 nm thick STO/Si film was reported by Woicik et al.26 Although we do not have a reliable estimate of the tetragonality, piezoresponse force microscopy on the 4.5 nm sample confirmed that RT ferroelectricity.

The tetragonality increase is attributed to Coulomb repulsion between atoms around V_0 .²³ The two electrons associated with a removed O atom are mainly localized on the $3d(z^2)$ orbital of the two neighboring Ti atoms, effectively replacing one Ti⁺⁴ atom with two Ti⁺³ and thus increasing the Ti ionic radius and c as well as the tetragonal distortion, c/a. Similar trends have been predicted computationally through Density Functional Theory (DFT), ^{28,29} consistent with our results. Sr/Ti non-stoichiometry could also lead to a change in c. It is difficult to disprove the existence

of a small amount of non-stoichiometry even in homoepitaxial STO thin films³⁰ and is especially problematic in PLD³¹ growth compared to MBE³² since the deposition rates of Sr and Ti cannot be independently controlled.

The dielectric functions of semiconductors change significantly with strain, 33 doping, 34 quantum confinement, $^{35-37}$ etc. Therefore, the increase in c and strain with V_O is expected to affect the electronic structure of STO/Si. To observe this change, SE was used to measure the films' dielectric function.

The optical properties of the Si substrates (from the same wafer batch used for the STO/Si films) and a STO bulk crystal were also measured by SE. A wavelength by wavelength approach was used to model the Si substrate layer and to allow for the extraction of the optical properties of the STO film from a least square regression analysis and an unweighted error function. The data were analyzed as ambient/film/substrate model, and the optical constants of STO were fitted. Fig. 3 shows the real, ε_1 , and imaginary, ε_2 , parts of the complex pseudodielectric function, $\varepsilon = \varepsilon_1 + i\varepsilon_2$ for three of the STO/Si samples, including the fits to the Tauc-Lorentz (TL) model (black line). This pseudodielectric

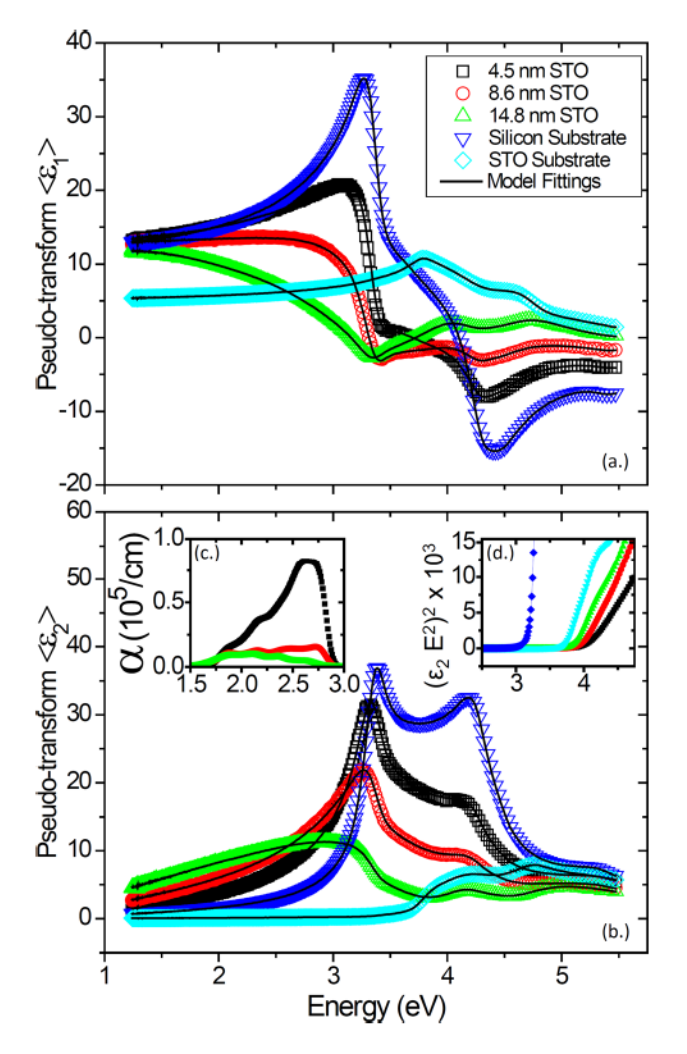


FIG. 3. As measured complex dielectric function and fits to the TL model (black line) for Set A, and bulk Si and STO. (a) ε_1 , and (b) ε_2 . (c) Absorption coefficient, α , around 2.6 eV for just the STO films. (d) Onset of absorption for the three films after removing the substrate optical properties through modeling. $(\varepsilon_2 E^2)^2$ vs. E is linear as expected for a direct optical transition.

function represents the as-measured dielectric properties of the film/substrate stack prior to modeling and therefore includes the interference fringes resulting from the interface observed as an increase in absorption with d at lower energy (Fig. 3(b)). A sum of TL oscillators can be used to fully describe the optical properties of the films. The TL oscillators, typically used for amorphous semiconductors and thin films, consist of a Lorentz function multiplied by a step function³⁸ to denote the absorption at the band gap edge and gave us the best fit compared to all other models. The mean squared error (MSE) was <3.0. The SE data were fitted well using only two TL oscillators. We also used models that accounted for graded compositions and interfacial layers but were found to be insignificant in improving the MSE. Including an effective medium Bruggeman model did not alter the results as expected, which agrees with our TEM data that do not show a SiO_x layer at the interface as opposed to other reports 16 that observe an effect of the interfacial SiO_x layers. The d of the films as determined by XRR and SE were similar, evidencing the correctness of our fitting procedure. An indirect band gap energy of 3.25 eV was measured for bulk STO but for the thin films the optical absorption is very weak. Attention was focused on the strong absorption edge of E_{di} around 3.7 eV. The onset of this strong absorption ranges from $3.86-4.2\,\mathrm{eV}$ depending on both d and V_{O} . Additionally, STO also has a critical point at 4.7 eV that can be seen in our data for thicker films.

For a semiconductor, near the absorption onset for the lowest, direct transition energy, E_{di} , the absorption spectrum versus photon energy, E is given by $\alpha(E)n(E)E \propto (E-E_{di})^{1/2}$ for $E>E_{di}$, where $\alpha=4\pi k/\lambda$ is the absorption coefficient equivalent to $\varepsilon_2 E^2 \propto (E-E_{di})^{1/2}$ (Tauc Law), ³⁹ consistent with our findings. Fig. 3(d) shows a plot of $(\varepsilon_2 E^2)^2 vsE$ just for the STO layer of Set A, near the vicinity of the bulk STO E_{di} of 3.75 eV. The plot is linear, as expected, even for the thinnest film, and from the extracted intercept E_{di} is calculated for both sets of films. The critical point analysis using Eq. (1) for expressing the dielectric function of the films is valid for three dimensions according to the dimensions of the wave vectors that participate in the optical transitions. Since we are measuring ultra-thin films, we also plotted $e^{\varepsilon_2 E^2} vs. E$ using the 2-D expression $\varepsilon_2 E^2 \propto ln(E-E_g)$, but the plot was non-linear. ³²

Fig. 2(a) (right axis) shows the extracted E_{di} as a function of d for Set A, where Fig. 3(b) shows a plot of E_{di} as a function of the $P(O_2)$ for Set B. E_{di} decreases from 4.10 ± 0.02 eV for the thinnest film of 4.5 nm to 3.85 ± 0.03 eV for the d = 30 nm, closer to the bulk measured value of 3.73 ± 0.02 eV. The indirect band gap around 3.20 ± 0.12 eV can also be observed for the thicker films but is much weaker, and a d dependence study was not attainable.

The blueshift of the band gap can be attributed to the effects of the increased strain for the thinner STO films. It has been reported that 13 nm thick STO films grown on KaTaO₃ substrates under a 2.2% (at max) biaxial tensile strain exhibit a blueshift in E_g of 230 meV compared to bulk STO. Our E_{di} are in agreement with calculations I predicting that under ~2% compressive biaxial strain and the associated ferroic distortions, the STO indirect band gap blueshifts and widens by $\approx 0.2 \, \mathrm{eV}$, comparing well to the

 $0.25 \,\mathrm{eV}$ widening of the E_{di} that we extracted. According to DFT calculations, ⁴¹ as the symmetry of the tetragonal phase is lowered compared to the cubic phase, conduction (primarily Ti 3d) and valence (primarily O 3d) states are allowed to mix and repel each other, and thus, the STO band gap is widened through new orbital mixing. A blueshift in the band gap has been observed as the strain increased in other systems such as in CdTe/GaAs layers where the value of the critical point energy-shift increased linearly. ⁴²

A smaller blueshift of the E_{di} with increasing V_O was measured for Set B as shown in Fig. 2 (bottom, right axis). This decrease of E_{di} with $P(O_2)$ correlates well with the smaller, as compared to Set A, change in c but can also be attributed to the decrease of the electron concentration as the amount of Vo decreases due to the Burstein-Moss effect, a blueshift of the E_{di} with increasing doping level after partially filling the conduction band with electrons. For Set A, we measured $n_s \approx 5.4 \times 10^{13} \, \text{cm}^{-2}$, roughly independent of d as expected, so the blueshift cannot be attributed to the Burstein-Moss effect. For Set B, since the carrier concentration increases with the amount of Vo, a Burstein-Moss effect cannot be ruled out. Nevertheless, the contribution of the electrons on the conductivity would also appear in the SE data as an increase of k at low energies (described by Drude theory) that was not observed in the data.

An intriguing feature of the STO optical spectrum is a broad, strong absorption peak $(0.8 \times 10^5 \,\mathrm{cm}^{-1})$ centered around 2.7 eV that is especially prominent for all films with $d < 6 \,\mathrm{nm}$ (only the 4.5 nm film is shown in Fig. 3). The increase in the absorption coefficient around 2.7 eV with a sharp cutoff is consistent with the reports of blue light emission around 2.9 eV observed in the photoluminescence emission spectra of Ar⁺ irradiated single crystal STO samples and oxygen deficient STO films grown epitaxially on undoped STO and was shown to correlate to the metallic nature caused by oxygen deficiency⁸ and Ti³⁺ formation.⁴³ Moreover, strong absorption has been observed from oxygen deficient STO films²³ below 3.2 eV, and has been attributed to the formation of defect states due to Vo that appear as a shallow defect level just below the conduction band and transition metals substituting for Ti3+ produce various opticalabsorption bands below the absorption edge of STO.⁴⁴ It has also been calculated that the electronic band structure for an oxygen-vacancy STO(001) Ti-terminated surface, some conduction band Ti 3d states cross the surface and become occupied, and the surface becomes metallic.38 Since the volume charge carrier and Vo concentration are lowest for the thin films, we would expect the 2.7 eV absorption peak to persist for the thicker samples. Another possibility is quantum confinement. SE has been successfully used in ultrathin (d < 10 nm) silicon-on-insulator³⁵ films for critical point analysis and to show that dimensional confinement in Si increases the E_1 transition energy by 75 meV compared to bulk Si. 45 A conduction band offset of ≈ 0.1 eV between p-Si and STO has been reported46 so the electrons in the thinner samples may experience dimensional confinement effects due to this potential barrier for electrons from STO to Si that may be amplified by ferroelectricity. The origin of this strong absorption will be further investigated.

We provide experimental evidence that the optical response of ultrathin STO films on Si is altered through either doping or strain engineering and that the shift of E_{di} has a quantifiable dimensional and doping dependence that correlates with the changes in crystal structure. Understanding the physics behind dimensional or doping changes in the dielectric function has both fundamental and practical applications as the desired optical properties can be engineered by designing the structure or the optical properties can be used to determine the oxygen deficiency.

This work was funded by the National Science Foundation (NSF) under a Career Award No. DMR-1255629.

¹A. Ohtomo and H. Y. Hwang, Nature **427**, 423 (2004).

²J. Biscaras, N. Bergeal, A. Kushwaha, T. Wolf, A. Rastogi, R. C. Budhani, and J. Lesueur, Nat. Commun. 1, 89 (2010).

³S. Stemmer and A. J. Millis, MRS Bull. 38, 1032 (2013).

⁴W. Maus-Friedrichs, M. Frerichs, A. Gunhold, S. Krischok, V. Kempter, and G. Bihlmayer, Surf. Sci. 515, 499 (2002).

⁵M. A. Saifi and L. E. Cross, Phys. Rev. B 2, 677 (1970).

⁶H. P. Frederik and W. R. Hosler, *Phys. Rev.* **161**, 822 (1967).

⁷O. N. Tufte and P. W. Chapman, Phys. Rev. **155**, 796 (1967).

⁸D. S. Kan, T. Terashima, R. Kanda, A. Masuno, K. Tanaka, S. C. Chu, H. Kan, A. Ishizumi, Y. Kanemitsu, Y. Shimakawa, and M. Takano, Nat. Mater. 4, 816 (2005).

⁹R. Al-Hamadany, J. P. Goss, P. R. Briddon, S. A. Mojarad, M. Al-Hadidi, A. G. O'Neill, and M. J. Rayson, J. Appl. Phys. 113, 024108 (2013).

¹⁰J. W. Reiner, A. M. Kolpak, Y. Segal, K. F. Garrity, S. Ismail-Beigi, C. H. Ahn, and F. J. Walker, Adv. Mater. 22, 2919 (2010).

¹¹B. K. Moon and H. Ishiwara, Jpn. J. Appl. Phys., Part 1 33, 1472 (1994).

¹²Z. Yu, Y. Liang, H. Li, J. Curless, C. Overgaard, R. Droopad, Y. Wei, X. Hu, B. Craigo, J. Finder, K. Eisenbeiser, A. Talin, S. Smith, S. Voight, J. Wang, D. Marshall, D. Jordan, J. Edwards, and K. Moore, *Crystalline Oxide-Silicon Heterostructures and Oxide Optoelectronics* (Materials Research Society, 2003), Vol. 747, p. 31.

¹³J. H. Haeni, C. D. Theis, and D. G. Schlom, J. Electroceram. 4, 385 (2000).

N. Warusawithana, C. Cen, C. R. Sleasman, J. C. Woicik, Y. Li, L. Fitting Kourkoutis, J. A. Klug, H. Li, P. Ryan, L.-P. Wang, M. Bedzyk, D. A. Muller, L.-Q. Chen, J. Levy, and D. G. Schlom, Science 324, 367 (2009).
S. Kim, D. J. Kim, T. H. Kim, T. W. Noh, J. S. Choi, B. H. Park, and J.-G. Yoon, Appl. Phys. Lett. 91, 042908 (2007).

¹⁶S. Zollner, A. A. Demkov, R. Liu, P. L. Fejes, R. B. Gregory, P. Alluri, J. A. Curless, Z. Yu, J. Ramdani, R. Droopad, T. E. Tiwald, J. N. Hilfiker, and J. A. Woollam, J. Vac. Sci. Technol. B 18, 2242 (2000).

¹⁷Y. Tian, C. Adamo, D. G. Schlom, and K. S. Burch, Appl. Phys. Lett. 102, 041906 (2013).

¹⁸Y. Wei, X. M. Hu, Y. Liang, D. C. Jordan, B. Craigo, R. Droopad, Z. Yu, A. Demkov, J. L. Edwards, and W. J. Ooms, J. Vac. Sci. Technol. B 20, 1402 (2002).

¹⁹H. Li, X. Hu, Y. Wei, Z. Yu, X. Zhang, R. Droopad, A. A. Demkov, J. Edwards, K. Moore, W. Ooms, J. Kulik, and P. Fejes, J. Appl. Phys. 93, 4521 (2003).

²⁰M. Wormington, D. K. Bowen, and B. K. Tanner, MRS Proc. 238, 119 (1992).

²¹L. G. Parratt, Phys. Rev. **95**, 359 (1954).

²²G. Niu, B. Vilquin, J. Penuelas, C. Botella, G. Hollinger, and G. Saint-Girons, J. Vac. Sci. Technol. B 29, 041207 (2011).

²³Y. S. Kim, J. Kim, S. J. Moon, W. S. Choi, Y. J. Chang, J.-G. Yoon, J. Yu, J.-S. Chung, and T. W. Noh, Appl. Phys. Lett. **94**, 202906 (2009).

²⁴A. Spinelli, M. A. Torija, C. Liu, C. Jan, and C. Leighton, Phys. Rev. B 81, 155110 (2010).

²⁵H. L. Cai, X. S. Wu, and J. Gao, Chem. Phys. Lett. **467**, 313 (2009).

²⁶J. C. Woicik, H. Li, P. Zschack, E. Karapetrova, P. Ryan, C. R. Ashman, and C. S. Hellberg, Phys. Rev. B 73, 024112 (2006).

²⁷A. Antons, J. B. Neaton, K. M. Rabe, and D. Vanderbilt, Phys. Rev. B 71, 024102 (2005).

²⁸J. Carrasco, F. Illas, N. Lopez, E. A. Kotomin, Y. F. Zhukovskii, R. A. Evarestov, Y. A. Mastrikov, S. Piskunov, and J. Maier, Phys. Rev. B 73, 064106 (2006).

- ²⁹C. Mitra, C. Lin, J. Robertson, and A. A. Demkov, Phys. Rev. B 86, 155105 (2012).
- ³⁰J. M. LeBeau, R. Engel-Herbert, B. Jalan, J. Cagnon, P. Moetakef, S. Stemmer, and G. Brian Stephenson, Appl. Phys. Lett. 95, 142905 (2009).
- ³¹T. Ohnishi, M. Lippmaa, T. Yamamoto, S. Meguro, and H. Koinuma, Appl. Phys. Lett. 87, 241919 (2005).
- ³²C. M. Brooks, L. Fitting Kourkoutis, T. Heeg, J. Schubert, D. A. Muller, and D. G. Schlom, Appl. Phys. Lett. 94, 162905 (2009).
- ³³A. Dejneka, M. Tyunina, J. Narkilahti, J. Levoska, D. Chvostova, L. Jastrabik, and V. A. Trepakov, Phys. Solid State 52, 2082 (2010).
- ³⁴M. Choi, A. B. Posadas, C. A. Rodriguez, A. O'Hara, H. Seinige, A. J. Kellock, M. M. Frank, M. Tsoi, S. Zollner, V. Narayanan, and A. A. Demkov, J. Appl. Phys. 116, 043705 (2014).
- ³⁵J. Price and A. C. Diebold, J. Vac. Sci. Technol. B **24**, 2156 (2006).
- ³⁶R. P. Vasquez, R. T. Kuroda, and A. Madhukar, J. Appl. Phys. 61, 2973 (1987).
- ³⁷C. Lin, A. Posadas, M. Choi, and A. A. Demkov, J. Appl. Phys. 117, 034304 (2015).

- ³⁸M.-Q. Cai, Y.-J. Zhang, G.-W. Yang, Z. Yin, M.-S. Zhang, W.-Y. Hu, and Y.-G. Wang, J. Chem. Phys. **124**, 174701 (2006).
- ³⁹H. G. Tompkins and E. A. Irene, *Handbook of Ellipsometry* (William Andrew, Springer, Norwich, New York; Heidelberg, Germany, 2005), p. 870
- ⁴⁰M. Tyunina, J. Narkilahti, J. Levoska, D. Chvostova, A. Dejneka, V. Trepakov, and V. Zelezny, J. Phys. Condens. Matter 21, 232203 (2009).
- ⁴¹R. F. Berger, C. J. Fennie, and J. B. Neaton, Phys. Rev. Lett. **107**, 146804 (2011).
- ⁴²M. S. Han, T. W. Kang, and T. W. Kim, Solid State Commun. 105, 709 (1998).
- ⁴³E. G. Rogers and P. Dorenbos, J. Lumin. **153**, 40 (2014).
- ⁴⁴K. W. Blazey, M. Aguilar, J. G. Bednorz, and K. A. Muller, Phys. Rev. B 27, 5836 (1983).
- ⁴⁵V. K. Kamineni and A. C. Diebold, Appl. Phys. Lett. 99, 151903 (2011).
- ⁴⁶S. A. Chambers, Y. Liang, Z. Yu, R. Droopad, and J. Ramdani, J. Vac. Sci. Technol. A 19, 934 (2001).